Title: Inactivation mechanism and efficacy of grape seed extract for Human Norovirus surrogate

Running title: Grape seed extract inactivates Tulane viruses

Chamteut Oh[1,*], Ratul Chowdhury[2,*], Laxmicharan Samineni[3], Joanna L Shisler[4], Manish Kumar[6], and Thanh H. Nguyen[1,5]

[1]Department of Civil and Environmental Engineering, University of Illinois at Urbana-Champaign, USA
[2]Department of Chemical Engineering, The Pennsylvania State University, PA, USA
[3]Department of Chemical Engineering, The University of Texas at Austin, Austin, USA
[4]Department of Microbiology, University of Illinois at Urbana-Champaign, USA
[5]Institute of Genomic Biology, University of Illinois at Urbana-Champaign, USA
[6]Department of Civil, Architectural and Environmental Engineering, The University of Texas at Austin, Austin, USA

[*]*Equal contribution*
Corresponding author(s): Thanh H. Nguyen (thn@illinois.edu)

Abstract

Proper disinfection of harvested food and water is critical to minimize infectious disease. Grape seed extract (GSE), a commonly used health supplement, is a mixture of plant-derived polyphenols. Polyphenols possess anti-microbial and -fungal properties, but anti-viral effects are not well-known. Here we show that GSE outperformed chemical disinfectants (e.g., free chlorine and peracetic acids) in inactivating Tulane virus, a human norovirus surrogate. GSE induced virus aggregation, an event that correlated with a decrease in virus titers. This aggregation and disinfection was not reversible. Molecular docking simulations indicate that polyphenols potentially formed hydrogen bonds and strong hydrophobic interactions with specific residues in viral capsid proteins. Together, these data suggest that polyphenols physically associate with viral capsid proteins to aggregate viruses as a means to inhibit virus entry into the host cell. Plant-based polyphenols like GSE are an attractive alternative to chemical disinfectants to remove infectious viruses from water or food.

Keywords: polyphenols; grape seed extract; Human norovirus surrogate Tulane virus; virus aggregation; Molecular docking simulations

Importance

Human noroviruses are major food- and water-borne pathogens, causing approximately 20% of all cases of acute gastroenteritis cases in developing and developed countries. Proper sanitation or disinfection are critical strategies to minimize human norovirus-caused disease until a reliable vaccine is created. Grape seed extract (GSE) is a mixture of plant-derived polyphenols that is used as a health supplement. Polyphenols are known for antimicrobial, antifungal, and antibiofilm activities, but antiviral effects are not well-known. In studies here, plant-derived polyphenols outperformed chemical disinfectants (e.g., free chlorine and peracetic acids) in inactivating Tulane virus, a human norovirus surrogate. Based on data from additional molecular assays and molecular docking simulations, the current model is that the polyphenols in GSE bind to the Tulane virus capsid, an event that triggers virion aggregation. It is thought that this aggregation prevents Tulane virus from entering host cells.

Introduction

Human noroviruses cause approximately 20% of all cases of acute gastroenteritis in developing and developed countries (1). In the United States, human noroviruses cause about 5.5 million cases of food borne illnesses per year, and about 2 billion dollars in economic loss (2, 3). Noroviruses are transmitted primarily by the fecal-oral route, including ingestion of contaminated food and water or via person-to-person contacts (4). Thus, inactivating human noroviruses present in contaminated food or water is important.

Sodium hypochlorite (NaClO) is regarded as the cheapest and most effective disinfectant to inactivate noroviruses on produce surfaces (5), stainless steel surfaces (6), or in liquid solutions (7). Fresh and fresh-cut produce are generally sanitized with residual chlorine concentrations of 50-200 μg/mL (8). Unfortunately, NaClO is toxic, and produces carcinogenic disinfection by-products (9–11). Thus, both consumers and industry are seeking methods to naturally or minimally process foods with minimal/zero chemical additives (12, 13).

Plants and fruits synthesize polyphenols, chemicals that protect them against damage from external stresses such as infection. Grape seed extract (GSE) is a by-product of grape juice and wine production, and is mass-produced at an affordable price (14, 15). GSE already is sold as an FDA-approved health supplement (16). GSE polyphenols have antimicrobial effects (17) and are considered popular alternatives to chemical disinfectants. GSE possesses anti-viral activity against feline calicivirus (FCV-F9), murine norovirus (MNV-1), bacteriophage MS2, and hepatitis A virus (14, 18, 19). However, the mechanism of virus inactivation is unclear (16). This information is critical because, if GSE is to be used by industries as a natural disinfectant, then researchers must understand how GSE inactivates different types of viruses.

The objective of this study was to examine GSE-induced inactivation of Tulane virus, a surrogate for human norovirus. Tulane virus is an ideal surrogate for norovirus because of its structural similarities to human noroviruses (20–22). Thus, Tulane virus has been used to provide more information about potential inactivation of norovirus (7, 23–27). Once GSE disinfection was established, we identified the mechanism of this inactivation using both molecular assays and computer modeling. Studies showed that GSE's main disinfection action occurred due to virus aggregation. Molecular docking simulations identified potential interactions between GSE polyphenols and viral capsids. This study is the first observation that shows plant-derived polyphenols can outperform chemical disinfectants in safely and sustainably controlling water-borne and food-borne pathogens, and also provides the first mechanism for GSE-induced virus inactivation. Thus, GSE may be an attractive disinfectant for industry because of its safety, efficacy and lower impact on the environment.

Results

GSE outperforms chemical disinfectants by 3-$\log_{10}$ TV titer reduction

Fig. 1 shows results from the examination of disinfection properties of GSE against Tulane virus, using a range of different GSE concentrations, Tulane virus (TV) concentrations, and incubation times. For all experiments, GSE was incubated with purified TV. GSE activity was halted by the addition of FBS, and plaque-forming units (PFUs) were quantified as a measure of virus inactivation. We tested GSE concentrations ranging from 42 µg/mL to 678 µg/mL because similar GSE concentrations were shown to inactivate other enteroviruses (14, 18, 19).

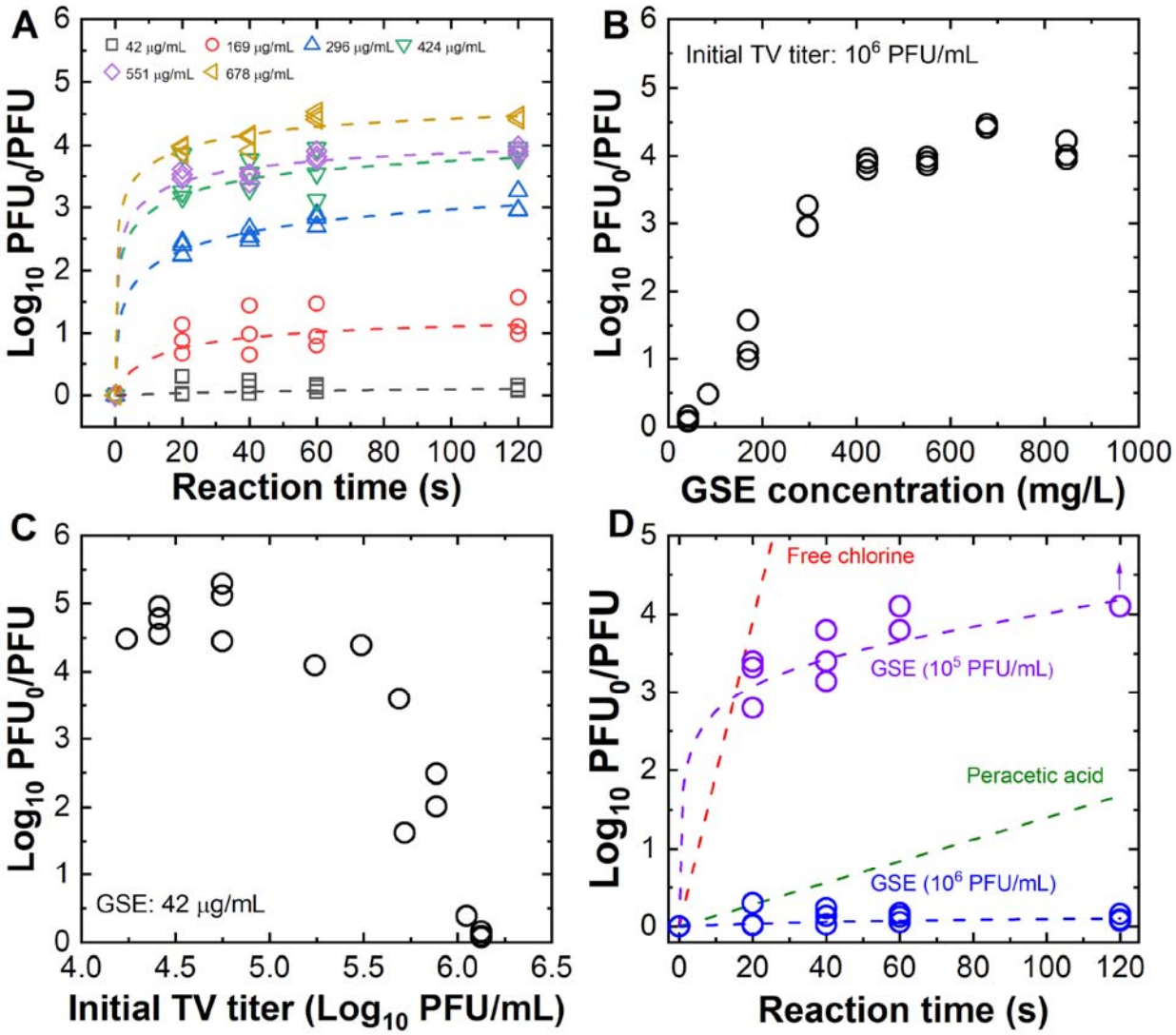

Fig. 1. Inactivation effects of GSE on Tulane virus. 10^6 PFU Tulane virus was incubated with the indicated amount of GSE. FBS was added to quench each reaction at the indicated times. Initial virus titer (PFU_0) was divided by the virus titer at each indicated time (PFU). Thus, the y-axis (Log_{10} PFU_0/PFU) indicates the decrease in virus titer caused by GSE on log_{10} scale. For all experiments, each symbol represents one molecular replicate. **(A)** The dashed lines were trend lines calculated by the pseudo-second-order model. TV inactivation as a function of GSE concentration and time. **(B)** TV inactivation as a function of GSE concentration. In this experiment 10^6 PFU TV was incubated for 120 seconds with the indicated GSE concentrations. **(C)** TV inactivation as a function of GSE concentration. Varying amounts of TV (indicated on the x-axis) were added to reactions containing 42 μg/mL GSE. All reactions were quenched with FBS after a 120 second incubation. **(D)** A comparison of GSE versus peracetic acid and free chlorine inactivation. 10^5 or 10^6 PFU TV was incubated with GSE (42 μg/mL) for 120 sec. The trend lines for GSE were determined by the pseudo-second-order model. The arrow indicates a detection limit. Trend lines for 42 μg /mL free chlorine or peracetic acid were derived by Chick's law with the rate constants determined by our previous studies(7, 27).

TV inactivation increased when GSE concentration and duration of incubation increased (**Fig. 1A**). The inactivation curves were fitted to both the pseudo-second-order model and Chick's law. The correlation coefficients (R^2 values), which reflect the goodness of fit, obtained by the pseudo-second-order model (0.99 to 1.00) were higher than those by the Chick's law (0.34 to 0.54) except for the lowest GSE concentration (42 μg/mL) where no significant reduction in virus titers was detected (one-way ANOVA, $p>0.05$). Parameters from the inactivation kinetics experiments are also listed in **Supplementary Table 1**. The fitting to the pseudo-second-order model showed that it took less than 120 seconds to reach a 95% of $\log_{10}$ PFU reductions at equilibrium state (i.e., $t_{95}<120$ seconds) for all tested conditions except for the 42 μg/mL case.

In **Fig. 1A**, better fitting achieved by the pseudo-second-order model suggested that chemisorption is the dominant reaction between the polyphenols and virus particles (28–30). This finding suggested there were optimal GSE:virion ratios for disinfection, as supported by data in **Fig. 1B** and **1C**. **Fig. 1B** showed that TV inactivation increased as GSE concentrations increased, with GSE efficacy reaching a plateau at 424 μg/mL. This plateau in GSE efficacy shows a maximal number of GSE binding sites on TVs because GSE disinfection could be outcompeted by the addition of TV. **Fig. 1C** showed that GSE disinfection efficiency decreased when more TVs were added to a reaction, supporting the hypothesis that chemisorption occurs between GSE and TV. Interestingly, while 42 mg/mL GSE showed no disinfection activity for 10^6 PFU TV (in **Fig. 1A**), it does indeed possess anti-viral properties when lower numbers of TV are present, further supporting the model that GSE polyphenols associate with TV.

We compared GSE inactivation rates to those of two commercially available chemical disinfectants (free chlorine and peracetic acid) based on Chick's law and the rate constants obtained from a previous study (27) (**Fig. 1D**). GSE inactivated TV to a 3-$\log_{10}$ virus titer

reduction within 16 seconds, a time identical to that of inactivation by free chlorine. In contrast, peracetic acid took much longer (211 seconds) to achieve the same levels of inactivation.

GSE causes viral aggregation, and this is likely the main mechanism of GSE-induced virus inactivation

Fig. 1 data showed that GSE inactivated TV, and data suggested that there was chemisorption of GSE to virions. Thus, one possibility is that GSE binds directly to TV to prevent virus-host interactions. **Fig. 2A** quantifies GSE polyphenols in the absence or presence of TV as a means to examine if GSE indeed binds to TV. We incubated 847 μg/mL GSE with 10^6 PFU TV. The 2 mL mixture then subjected to ultracentrifugation to separate free versus virus-bound GSE, and GSE in supernatants of samples were quantified. As shown in **Fig. 2A**, there was a statistically significant lower GSE concentration in supernatants when TV was present, implying that GSE indeed binds to TV. Next, we used a light scattering analyzer (DelsaMax Pro, Beckman Coulter) to examine particle size distributions of intact TV and GSE (**Fig. 2B)**. Untreated TV showed a polydispersed multimodal size distribution with a major peak at 97 nm and two relatively smaller peaks at 309 and 1755 nm. A single TV virion has a diameter of 40 nm (31), thus most of the TVs in solution were present as dimers, and some populations of viruses were present as timers. Virus populations at 1755 nm were likely multi-virus aggregates. When TV was incubated with 15 μg /ml GSE, there was a shift in the size of the TV peak at 94 nm to approximately 300 nm and 1000 nm, implying that this concentration of GSE causes aggregation of TV into trimers and perhaps 10-mers. Experiments using higher concentrations of GSE resulted in greater shifts in sizes, suggesting that GSE is causing TV aggregation. GSE showed a strong single peak at around 1000 nm regardless of GSE concentrations. This peak is

believed to represent insoluble polyphenols that are self-aggregated (32). When the GSE solutions were filtered with 0.1 μm filter, the monodispersed peak disappeared from the particle size distribution.

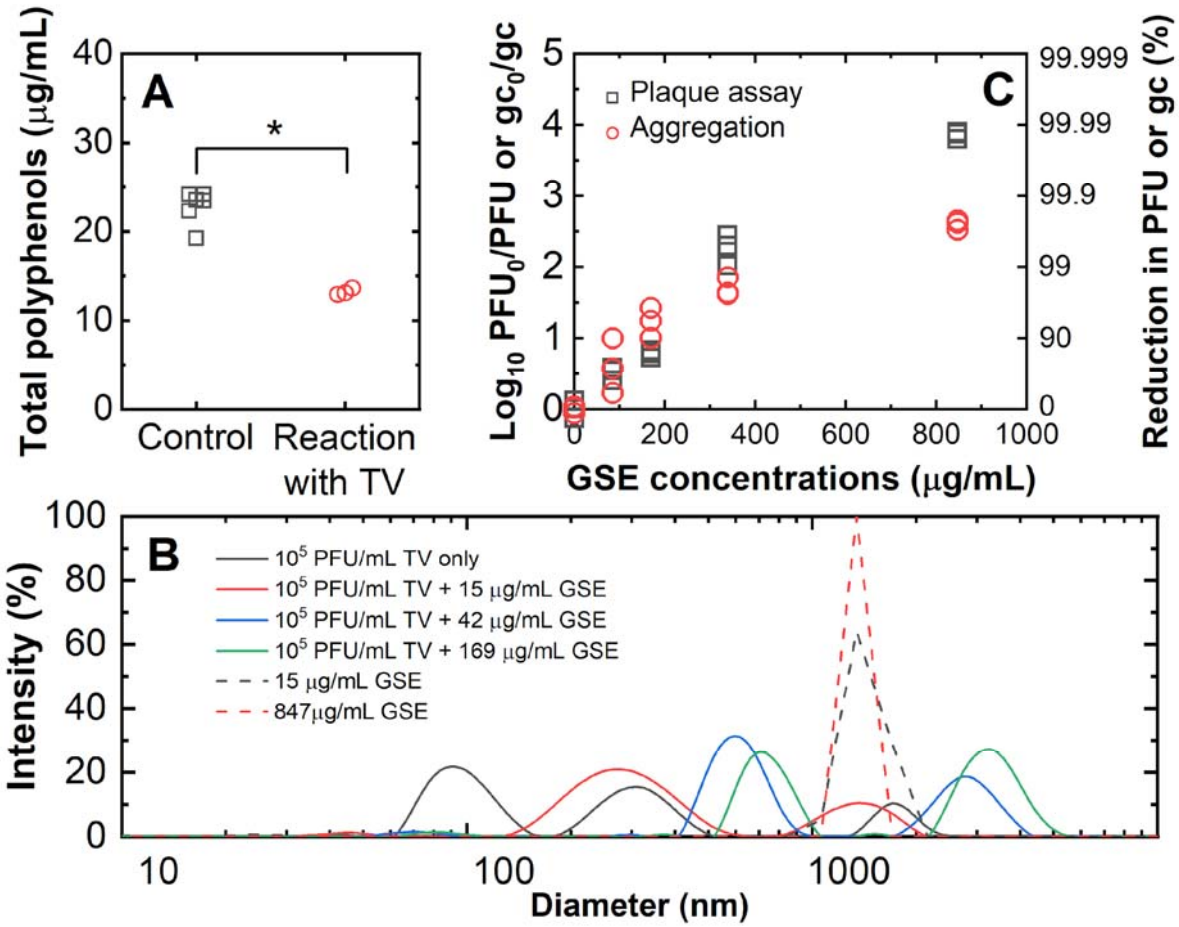

Fig. 2. GSE-induced TV aggregation. (A) Solutions either lacking (control) or containing 10^6 PFU TV were each incubated with 847 μg/mL of GSE followed by ultracentrifugation (150700 g) for 3 hours. GSE concentrations were quantified and statistical analysis was performed using the Mann-Whitney test ($P<0.05$) **(B)** The particle size distribution of TV in the presence or absence of GSE. **(C)** A dose-response curve for plaque and aggregation assays. Plaque assay results were normalized to the initial virus titer and presented in Log_{10} PFU_0/PFU to indicate the decrease in virus titer with different total polyphenol concentrations. Aggregation assay was analyzed by the one-step RT-qPCR and presented in the normalized gene copy number (Log_{10} gc_0/gc) to show the reduction in the number of virions. Equivalent reductions in PFU or gc (%) were also presented on the right y-axis for plaque assay and aggregation assay, respectively. For these experiments, 10^6 PFU TV was incubated with varying concentrations of GSE for 2 minutes

188 followed by quenching the reaction with FBS. Each symbol indicates one separate experiment
189 where one plaque assay or three qPCR analyses were conducted.
190

191

192 To further test if GSE induces virus aggregation, virus aggregation and virus titers were
193 quantified in parallel to compare the numbers of virus aggregates and inactivated virus particles
194 after the GSE treatment. For assays shown in **Fig. 2C**, 10^6 PFU TV was incubated with the
195 indicated concentrations of GSE (85 to 847 μg/mL) for 2 minutes followed by quenching the
196 reaction with FBS. Viruses were then either quantified by plaque assay or tested using an
197 aggregation assay. Aggregation assays were designed as follows: untreated or GSE-treated TV
198 were subjected to filtration using a 0.1 μm sized pore filter. Because a single TV virion has a
199 diameter of 40 nm (31), we expect that single and dimeric TV would easily filter through the
200 pore while virus aggregates with three or more virions would be trapped in the filter. Note that
201 our aggregation assay cannot determine a specific number of virions in virus aggregates that can
202 pass through the filter. Viruses that passed through the filter were quantified by one-step RT-
203 qPCR. The ratio of genome copies for untreated versus treated viruses (Log_{10} gc_0/gc) were
204 plotted on the y-axis in **Fig. 2C**. Similar to **Fig. 1**, plaque assays measured virus titers in
205 untreated samples (PFU_0) versus GSE-treated samples (PFU), and data are presented as the ratio
206 of virus titers before and after exposure to GSE (Log_{10} PFU_0/PFU) on the y-axis in **Fig. 2C**.
207 Virus aggregates and plaque were very similar when GSE concentrations below 400 ng/ml were
208 used. However, virus aggregates were significantly lower than inactivated virus titers when 847
209 μg/mL GSE was present. This discrepancy shows the number of virus particles that are larger
210 than 0.1 μm does not fully explain the number of inactivated virus particles determined by the
211 plaque assay. Nevertheless, paired t-test revealed that there was no significant difference

between the plaque assay and aggregation assay results over the different GSE concentrations ($P>0.05$). Thus, our current model is that GSE interacts with TV capsid, causing TV aggregation. In turn, aggregation would likely prevent TV from entering host cells. We also demonstrate that GSE aggregation was not reversible; removal of GSE from TV-containing solutions did not make aggregated TV return back into single particle solutions (**Supplementary Text 1**).

Molecular docking indicated polyphenols strongly bound to capsid proteins

Data from **Fig. 2** indicated that GSE is physically associated with TV and induced virus aggregation, and that this event likely prevents TV from entering the host cell to begin the virus life cycle. To further investigate this possibility, we conducted molecular docking simulations, an approach that was used to identify interactions between polyphenolic compounds and proteins (33, 34). GSE is a mixture of various polyphenolic compounds (35, 36). We selected nine polyphenolic compounds present in GSE for molecular docking experiments. We chose these compounds based on abundance (36), and this included two phenolic acids (gallic acid and protocatechuic acid), three monomer flavan-3-ols (catechin, epicatechin, and epicatechin gallate), and four dimer flavan-3-ols based on LC-MS analysis (procyanidin B1, B2, B3, and B4) (**Supplementary Table 2**). Although we conducted inactivation experiments using TV, we could not perform molecular docking simulations with the TV capsid because there is no entry for the TV capsid in the Protein Data Bank (PDB, https://www.rcsb.org/). Cryo-EM analysis has shown similarity between the TV and human norovirus (HuNoV) capsids (31), and the HuNoV capsid structure is present in the PBD. Thus, we studied the interaction of the GSE polyphenols with the HuNoV VP1 capsid proteins to understand how GSE may interact with similar TV capsid proteins.

We performed flexible molecular docking simulations (37, 38) between each of the nine GSE polyphenolic compounds and HuNoV VP1 proteins to discern stable docking conformations, across the four domains of VP1 (S, S-P1 hinge, P1, and P2 domain; **Supplementary Fig. 2**) to identify where each of the polyphenols tended to bind in order of domain preference. For these simulations, we used the HuNoV icosahedral asymmetric unit (PDB ID: 1IHM) that comprised three VP1 proteins because the complete HuNoV capsid consists of 180 identical icosahedral asymmetric units. Residue-level domain definitions have been described by Campillay-Véliz et al. (39). Flexible molecular docking simulations are shown in **Fig. 3**. The expected binding strength of each polyphenol (in increasing order of size/molecular weight) with HuNoV capsid protein has been reported where the error bars indicate variance across top 15 polyphenol binding poses within the same capsid groove. The scale on the right indicates fractional capsid-binding affinity of a given polyphenol with respect to the positive control – BSA. Larger polyphenols tend to show increased affinity towards both the positive control and target capsid of HuNoV. Analysis of binding affinities from docking experiments reveal greater electrostatic stabilization of the larger conjugated electron systems within the bigger polyphenols by the polar grooves of HuNoV capsid and bovine serum albumin alike. Data demonstrated that each of the nine polyphenolic compounds examined from GSE likely bound to different residues or regions of the HuNoV capsid protein. In addition, these polyphenols appeared to bind to a location at the dimeric interface of the trimeric capsid protein. The scores obtained from the simulation reflect the enthalpic contribution of binding (kcal/mol) between the polyphenols and the capsid (40). Fifteen independent trajectories of docking were performed using the docking protocol from OptMAVEn-2.0 suite (38) and the Rosetta energy function (41) was used to score the docked poses. The expected binding score was reported to be

the modal value (i.e., most probable score) across the fifteen recorded values per complex. Since the polyphenols tend to show a conjugated electron system, larger polyphenols showed better electrostatic stabilization by the polar binding groove offered by the capsid proteins. Consequently, flavan-3-ol dimers showed stronger binding affinities to the capsid protein than smaller groups of polyphenols (**Fig. 3**). The polyphenol-capsid interaction profiles were composed primarily of hydrogen bonds along with hydrophobic interactions, accounting for the efficient capsid capture seen in experiments (**Fig. 4**). For example, the smallest polyphenol protocatechuate establishes three hydrogen bonded and three hydrophobic contacts while procyanidin (the largest polyphenolic compound) shows up to ten hydrogen bonded contacts yet maintaining the same number of hydrophobic interactions with the capsid (**Supplementary Fig. 3**). In addition to being concordant with a previous experimental study showing that polyphenols' binding affinity to proteins (e.g., BSA and human salivary α-amylase) increased with their molecular weights (42), we also provide key biophysical insights for the same in this work (**Fig. 4**). Binding affinities for respective polyphenols with the HuNoV capsid were near-equal to that of bovine serum albumin, our positive control (**Fig. 3**). The bovine serum albumin is known as the major protein in FBS (43), with reported quenching activity towards polyphenolic compounds. Thus, our results indicated that the GSE polyphenols tend to promote capture of viral capsids with high efficiency.

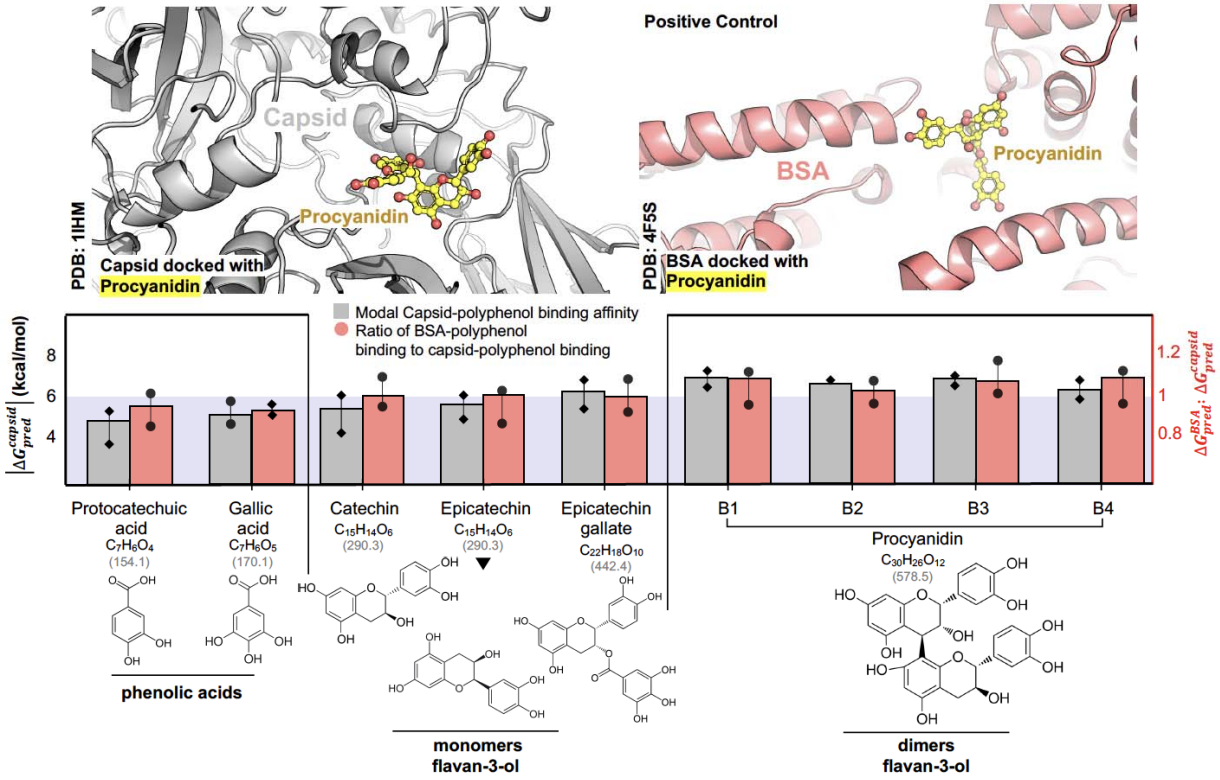

Fig. 3. Summary of molecular docking analysis between HuNoV capsid and GSE selected polyphenols found in GSE. BSA, which is known to bind strongly with polyphenols (14), was used as a positive control. The expected binding strength of each polyphenol (in increasing order of size/molecular weight) with HuNoV capsid protein (PDB id: 1IHM) has been reported where the error bars indicate variance across top 15 polyphenol binding poses within the same capsid groove. The scale on the right indicates fractional capsid-binding affinity of a given polyphenol with respect to the positive control – BSA.

A

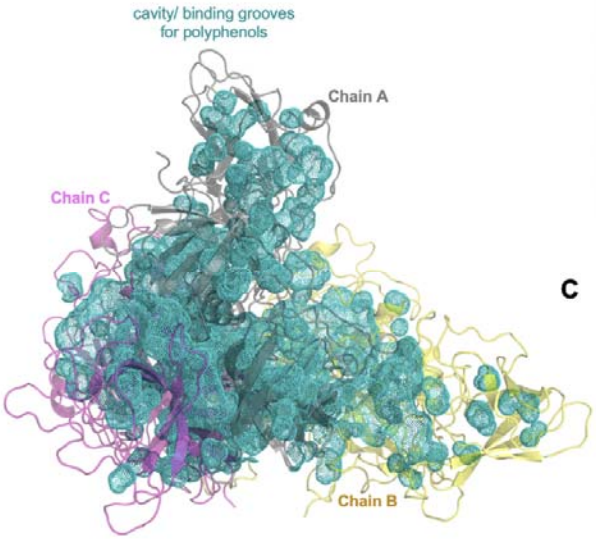

B

Hydrophobic Contacts			H-bonded interaction							
Res. Num	Res. Name	Distance (Å)	Res. Num	Res. Name	Distance (Å)	Donor Angle (°)	Res. Num	Res. Name	Distance (Å)	Donor Angle (°)
3084B	SER	3.79	3084B	SER	3.21	166.2	3174B	ASP	3.91	169.2
3178B	GLU	3.43	3088B	HIS	3.52	129.3	3175B	ARG	3.63	113.4
3506B	TRP	4.81	3103B	TRP	3.92	139.4	3453B	VAL	3.67	161.4
			3133B	GLY	2.96	117.5	3455B	GLU	4.01	125.4
			3134B	SER	3.21	143.0	3508B	SER	3.77	133.7

C

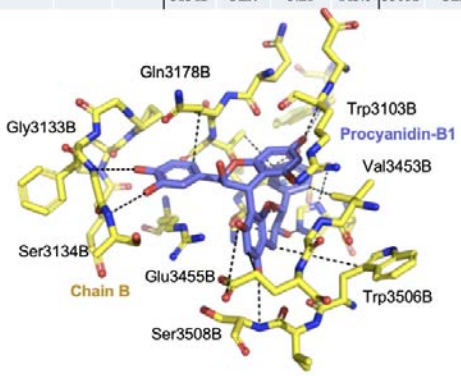

Fig. 4. Larger polyphenols show greater electrostatic stabilization with the viral capsid. **(A)** HuNoV capsid shows a trigonal-symmetric polyphenol accessible groove (indicated in teal), which includes three intra-chain pockets, and three inter-chain binding crevices. Smaller polyphenols can access the inter-chain crevices, while the bigger ones remain localized to the more solvent-exposed intra-chain pockets. **(B)** Residue level interactions of Procyanidin-B1 with the HuNoV capsid are listed. **(C)** A graphical overview of the exact docked pose of Procyanidin-B1 in the capsid groove with most of the interactions is illustrated.

It is noteworthy that as the size of the polyphenol increases, it tends to bind to a less-buried, more solvent exposed pocket (owing to steric clashes) (**Fig. 5**) yet binding to the interface of two chains of the trimeric capsid (located around the S-P1 hinge domain; **Supplementary Fig. 2**). Only the largest Procyanidin (B1-B4) polyphenols cannot access the inter-chain interface pockets and are primarily surface binders with most interactions limited to a single chain (**Fig. 5**). We thereby hypothesize that larger polyphenols tend to be surface binders but stronger capsid binders, while smaller ones preferably bind to inter-chain interfaces of the viral capsid. In terms of domains bound, our docking simulations, in concordance with the experimental data, show that most polyphenols bind to the S or S-P1 hinge domains - while trace binding is observed in the P1 domain and P2 domain is mostly unbound.

306

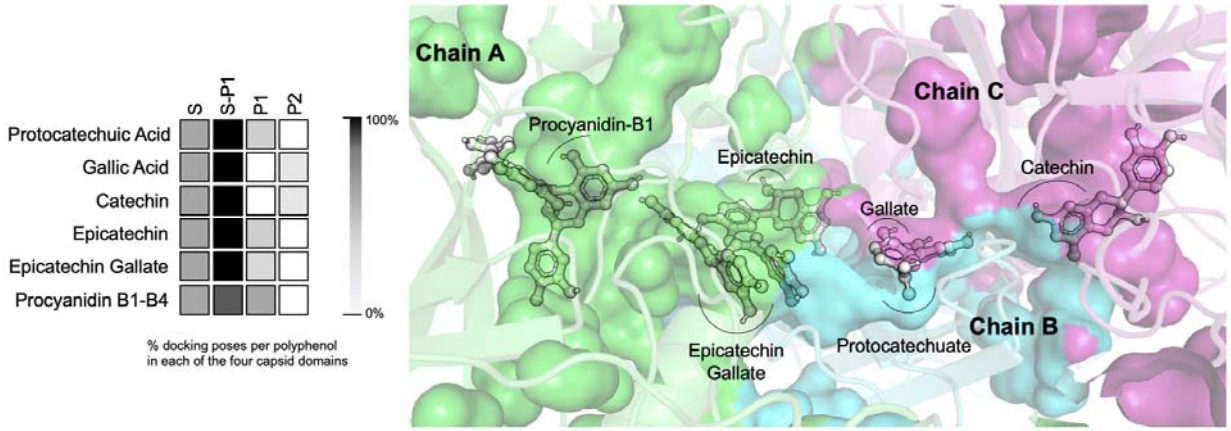

307

308 **Fig. 5**. All polyphenol binding is primarily localized around the S and S-P1 hinge domains of the
309 HuNoV capsid - while the P2 domain remains mostly unbound. Smaller polyphenols can access
310 more buried inter-chain pockets of the HuNoV capsid, while larger Procyanidins bind to surface-
311 exposed pockets with a single chain. Pockets guarded by each chain have been indicated by a
312 different color (green – A, cyan – B, magenta – C). Smaller polyphenols – protocatechuate,
313 gallate, and catechin bind best at the interface of chains B and C. Slightly larger epicatechin and
314 epicatechin gallate bind best at the interface of chain A and B, while larger procyanidins (all B1
315 through B4) bind best to a solvent-exposed cavity within chain A only.
316

317 We extended the molecular docking simulations to other enteric viruses such as feline
318 calicivirus (FCV-F9), murine norovirus (MNV-1), and hepatitis A virus (HAV) that were
319 experimentally studied in previous works (14, 18, 19). Although the three sets of experiments
320 were performed in different conditions such as different virus media (water or produce) and
321 different pH, they presented a similar trend that FCV-F9 is more susceptible to the polyphenols
322 in GSE than MNV-1 and HAV. Our molecular docking simulation agreed with the experimental
323 data with these enteric viruses. The binding energy of the polyphenols to FCV-F9 capsid protein
324 were stronger than those of MNV-1 and HAV ($P<0.05$) (**Fig. 6**). Note that the binding energy
325 alone will not be sufficient information to evaluate the antiviral effect of the polyphenols because

326 the binding energy does not necessarily indicate the following reactions such as viruses being
327 aggregated and losing infectivity.
328

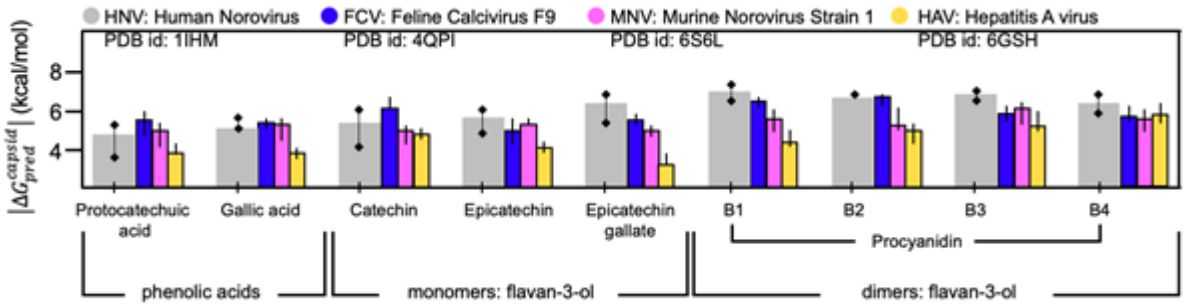

329

330 **Fig. 6.** Expected binding energies (absolute modal values) between each polyphenolic compound
331 and the four viral capsids (HuNoV: human norovirus, FCV: feline calicivirus F9, MNV: murine
332 norovirus strain 1, and HAV: hepatitis A virus) were computed using the Rosetta binding energy
333 function from top 15 docking poses per complex. The error bars indicate variance from the 15
334 docked poses for each complex. The reported energy scores were compared by a paired sample t-
335 test indicating a statistically significant higher polyphenol binding activity by HuNoV and FCV
336 in contrast to MNV ($P<0.05$) and HAV ($p<0.001$) capsids.
337

338 **Discussion**

339 Anti-bacterial, anti-biofilm, and anti-fungal effects of plant-derived polyphenols are well-
340 known. In this study, we systematically evaluated antiviral efficacy of the polyphenols in GSE to
341 TV, a surrogate virus for HuNoV, and the antiviral mechanisms. Data shown here suggest that
342 GSE can inactivate TV and perhaps other enteric viruses. In addition, data show that the
343 polyphenols in GSE aggregate the virus particles, an event that is likely responsible for TV
344 inactivation. Indeed, this concept that TV adsorbs polyphenols was also supported by the binding
345 energy calculated by molecular docking analysis. Our current model is that TV aggregation
346 prevents proper virus-host interactions or virus entry into host cells. There is at least one other
347 report of aggregation of herpes simplex virus, prevents virus entry into cells while allowing virus
348 attachment (44).

349 It should be noted that the TV concentrations used in this study are likely much higher
350 than that found in contaminated produce or water. For example, rotavirus concentration in river
351 water, treated wastewater, and untreated wastewater are reported to be $10^{-3.0}$,$10^{-2.2}$, and $10^{-1.3}$
352 FFU/mL respectively (45, 46). Given that GSE was efficacious using these artificially high TV
353 concentrations used in the laboratory, it is reasonable to expect that GSE would be effective as
354 an anti-viral for contaminated food or produce. Also, Tulane virus is more resistant to chemical
355 disinfectants than the other viruses in the *Caliciviridae* family (47). Thus, if GSE were an
356 effective disinfectant of Tulane virus then it is likely GSE would be efficacious against other
357 caliciviruses, and this is an avenue of future research. GSE is also attractive because it is safe for
358 consumption by humans. Thus, GSE or plant-derived polyphenols could be advantageous over
359 the chemical disinfectants for direct addition to end-products that people ingest such as drinking
360 water and foods.

361 There are still several important questions to answer before polyphenols can be widely
362 used to inactivate the water-borne and food-borne pathogens. Water contains other organic
363 matter which could outcompete viruses for binding to polyphenolic compounds. For example,
364 Joshi et al. (14) showed the antiviral efficacy decreased when milk (which has high proteins) was
365 added to an inactivation reaction. Thus, further studies need to be performed to understand how
366 effective GSE is in water that has different properties. Other water properties (e.g., pH, ionic
367 strength, and temperature) are important for adsorption reactions, and additional studies need to
368 address how these properties may affect the efficacy of GSE. If GSE or individual polyphenols
369 were to be used for foods (e.g., apples) then we must also understand how the surface properties
370 of foods (e.g., wax contents of produce surface) may affect the efficacy of GSE (27).
371

Materials and Methods

Commercially available grape seed extract and its plant-derived polyphenols

We purchased a commercial grape seed extract (GSE) solution for this research (7832, Natures plus, USA). The total polyphenol (TP) concentration in each GSE sample was quantified by the colorimetric method using Folin-Ciocalteu reagent. A mixture of 100 μL GSE sample and 500 μL of 10% Folin-Ciocalteu phenol reagent (Sigma-Aldrich, MO, USA) was prepared in a 10 mm path length polymethyl methacrylate (PMMA) cuvette (BrandTech Scientific, CT, USA). Within 3 to 8 min of mixture preparation, 400 μL of 7.5% sodium carbonate solution was added to the mixture and homogenized by pipetting. After incubating at room temperature for 60 minutes, UV absorbance at 765 nm was measured by a spectrophotometer (UV-2450, Shimadzu, Japan). Distilled water was used as a reference solution. The same procedure was conducted with gallic acid solutions with different concentrations prepared by diluting gallic acid monohydrate (Sigma-Aldrich, MO, USA) in distilled water. The TP concentrations of the gallic acid solutions were used for a calibration curve (**Supplementary Fig. 4**) which determined TP concentration of the GSE samples. GSE with TP concentrations ranging from 84 to 1694 μg/mL was prepared by diluting the initial GSE with 1X PBS and used for inactivation experiments.

The polyphenol composition of GSE was analyzed by liquid chromatography-mass spectrometry (Q Exactive™ Plus Hybrid Quadrupole-Orbitrap™ Mass Spectrometer, Thermo scientific, USA), and numerous peaks were discovered by untargeted comprehensive metabolite profiling (**Supplementary Table 2**). Although the LC/MS analysis could not quantify each polyphenol and differentiate polyphenolic isomers with the same m/z values, such as catechin/epicatechin at 291 of m/z ratio for $[M+H]^+$ and B type procyanidins at 579 of m/z ratio for $[M+H]^+$, the major peaks agreed with the primary polyphenolic compounds in GSE that were

confirmed by other studies (35, 36). With the mass spectrometry and the references characterizing polyphenols in GSE, we chose nine target polyphenolic components, which include three monomers flavan-3-ols (catechin, epicatechin, and epicatechin gallate), four dimers flavan-3-ols (Procyanidin B1, Procyanidin B2, Procyanidin B3, and Procyanidin B4), and two phenolic acid (gallic acid and protocatechuic acid). These nine polyphenolic compounds were further studied through molecular docking simulations.

Tulane virus propagation

Tulane virus (TV) was used as a surrogate for human norovirus (HuNoV). Both TV and HuNoV are members of *Caliciviridae* and share structural similarities. TV and HuNoV have a positive-sense, single-stranded genomic RNA of 6.7 kb and 7.5 kb, respectively. About 23-26% of the genome sequences are identical in both viruses (20). The capsid of TV has T=3 icosahedral symmetry and is 40 nm in diameter. The capsid comprises 180 copies of major capsid protein (VP1) or 90 dimers of A/B or C/C. The VP1 is also sub-divided into S, P1, and P2 domains. When the VP1 proteins are assembled, the S domains comprise the bottom surface of the capsid while P1 and P2 domains protrude out of the bottom surface, which is responsible for binding to receptor proteins (**Supplementary Fig. 1**). TV recognizes Histo-blood group antigens (21) and sialic acids (22) as cellular receptors similar to HuNoVs. Besides, TV is considered more resistant to disinfectants than the other viruses in *Caliciviridae* (47). Therefore, TV has been widely used in virus inactivation experiments as a surrogate for HuNoVs (7, 23–27).

TV was a gift from Cincinnati Children's Hospital Medical Center (22) and the TV genome was sequenced as quality control. The genome sequence was 100% identical to those of a wild-type TV strain in Genbank (Access number: EU391643) (7). TV was propagated in

MA104 cells, which was purchased from ATCC (CRL-2378.1), and grown in complete culture medium (i.e., 1X minimum essential medium (MEM; Thermo Fisher Scientific, USA), 10% fetal bovine serum (FBS; Thermo Fisher Scientific, USA), 1X antibiotic-antimycotic (Thermo Fisher Scientific, USA), 17 mM of $NaHCO_3$, 10 mM of HEPES, and 1 mM of sodium pyruvate (Thermo Fisher Scientific, USA). When greater than 90% of MA014 cellular monolayers showed cytopathic effects (about 2 days after the inoculation), cells were harvested and collected by centrifugation, and TV was released from host cells by three cycles of freeze and thaw. Virus was separated from cellular debris by centrifugation at 2000 rpm (556 g) for 10 min (Sorvall Legend RT Plus, Thermo Fisher Scientific, USA). The supernatant was treated by filtration with a 0.22 μm bottle top filter (Milliporesigma, USA) to remove additional cellular debris. The virus-containing filtrate was then further purified using an ultracentrifuge (Optima XPN-90 Ultracentrifuge, Beckman Coulter, USA) with a cycle of 1,000 rpm (116 g) for 5 min followed by 36,000 rpm (150700 g) at 4°C for 3 hours. The virus pellet was resuspended in 1X PBS, aliquoted, and stored at -80□ before use.

Tulane virus inactivation experiments using GSE

Virus inactivation experiments were initiated by adding 250 μL of TV solution containing 2.5 x10^5 PFU TV to 250 μL of GSE-containing solution, in which GSE concentrations ranged from 84 to 1694 μg/mL. After the incubation times indicated in the manuscript (i.e., 10 to 120 seconds), 70 μL of the mixture was added to 70 μL of FBS to quench the polyphenolic activity(14). Thus, the volumetric ratio of TV, GSE, and FBS in the final solution was 1:1:2. The FBS quenching activity was confirmed in **Supplementary Fig. 5**. Negative controls were prepared for every virus inactivation experiment. In this case, the negative controls were

441 prepared by mixing TV, GSE, and FBS in the ratio of 1:1:2, but in a different mixing order.
442 Specifically, 35 µL of GSE was mixed with 70 µL of FBS to quench the polyphenolic activity
443 followed by adding 35 µL of TV to the mixture (**Fig. 1A**). The final mixture of TV, GSE, and
444 FBS was used for further analysis.
445
446 **Plaque assays**
447 The MA104 cell line was grown in 175 cm^2 flasks (Thermo Fisher Scientific, USA) with the
448 complete culture medium. Cells were seeded into 6-well plates (CC7682-7506, USA Scientific,
449 USA) resulting in cellular monolayers with more than 90% confluency. Cell culture supernatants
450 were aspirated using a vacuum-connected pasteur pipette. 100 µL of TV samples were serially
451 diluted by 10-fold dilutions. Cellular monolayers were incubated with each of the serially-diluted
452 viruses for 1 hour at 37□ with 5% CO_2 to facilitate virus attachment to the MA104 cells. Viruses
453 were aspirated from cellular monolayers and 2 mL of overlay solution containing 1X MEM, 1%
454 agarose, 7.5% sodium bicarbonate, 15 mM HEPES, and 1X antibiotic-antimycotic was added to
455 each well. The overlay solution was solidified at 4□ for 10 minutes. Plates were incubated for 2
456 days at 37□ with 5% CO_2 to allow infectious viruses to form plaques. Next, 2 mL of 10%
457 formaldehyde (VWR, USA) in 1X PBS was added to each well and incubated at room
458 temperature for 1 hour to fix cells. The agarose and the formaldehyde were removed and
459 replaced with a 0.05% crystal violet dye solution. The solution was washed away after 10
460 minutes and the number of plaque-forming units (PFU) was counted on a lightbox (ULB-100,
461 Scienceware). The detection limit of the plaque assay was one plaque on the least diluted sample
462 (i.e., 10-fold dilution), which was equivalent to $10^{1.1}$ PFU/mL.
463

Models for virus inactivation kinetics

TV inactivation kinetics were interpreted by a first-order reaction of Chick's law (Eqs. 1-3) and pseudo-second-order model (Eqs. 4-6). Chick's law assumes the activity (i.e., concentration) of available disinfectant remains constant during the reaction. Chick's law has been widely used to describe virus inactivation kinetics by free chlorine, peracetic acid, monochloramine, heat, ozone, and UV(7, 48–51).

$$\frac{dN}{dt} = -kcN \qquad \text{(Eq. 1)}$$

$$ln\frac{N}{N_0} = -kct \qquad \text{(Eq. 2)}$$

$$log_{10}\frac{N_0}{N} = k'ct \qquad \text{(Eq. 3)}$$

Where *N* referred to viral infectivity (PFU/mL), *c* indicated the TP concentration (μg/mL), *t* was treatment time (s), *k'* meant an inactivation rate constant from Chick's law (L/μg·s).

The pseudo-second-order model has been widely used to describe reactions where chemisorption between adsorbent and adsorbate is the rate-determining step (28). In this study, TV and TP were considered as adsorbate and adsorbent, respectively.

$$\frac{dC_t}{dt} = k_2(C_e - C_t)^2 \qquad \text{(Eq. 4)}$$

$$\frac{t}{C_t} = \frac{1}{C_e^2 k_2} + \frac{1}{C_e}t \qquad \text{(Eq. 5)}$$

$$t_{95\%} = \frac{19}{C_e k_2} \qquad \text{(Eq. 6)}$$

Where t is the reaction time (s), k_2 is the rate constant from the pseudo-second-order model (mL/PFU·s), C_t and C_e are inactivated TV concentration (PFU/mL) at time t and equilibrium state, respectively. Also, $t_{95\%}$ is a reaction time at which C_t reaches 95% of C_e.

Virus particle size

The particle size distribution of TV was measured by a light scattering analyzer (DelsaMax Pro, Beckman Coulter). TV, GSE, and FBS either alone or in combination were prepared in 200 μL aliquots, placed in a PMMA cuvette (BrandTech Scientific, USA). Particle size was measured 20 times for each sample, and the averaged % intensity was presented with the particle diameter. According to the manufacturer, particle size analysis is reliable within a range from 0.4 to 10,000 nm, and all our measurements were in this detection range.

Virus aggregation assay

An assay was developed to quantify TV virions that are less than 100 μm in diameter. After the TV inactivation experiments were conducted, the mixture containing viruses, GSE, and FBS was filtered with a 0.1 μm syringe filter (Sartorius, Germany). The number of virus particles in the initial mixture and the filtrate was quantified by one-step RT-qPCR. RNA was extracted from samples using Viral RNA Mini Kit (QIAGEN, Germany) in a final 60 μL volume. RT-qPCR samples were prepared in 96-well plates (4306737, Applied Biosystems, USA) by mixing 5 μL of 2 × iTaq universal SYBR green reaction mix, 0.125 μL of iScript reverse transcriptase from the iTaq universal SYBR green reaction mix (Bio-Rad Laboratories, USA), 3 μL of the RNA, 0.3 μL of 10 μM TV-NSP1-qPCR-F primer, 0.3 μL of 10 μM TV-NSP1-qPCR-R primer, and 1.275 μL of nuclease-free water. The one-step RT-qPCR was run using a qPCR system (QuantStudio

3, Thermo Fisher Scientific, USA) with the following thermocycle: 10 minutes at 50□ and 1 minute at 90□ followed by 40 cycles of 30 seconds at 60□ and 1 minute at 90□. Detailed information for primers and synthetic DNA controls is summarized in **Supplementary Table 3**. We obtained a calibration curve by plotting the viral infectivity (Log_{10} PFU/mL) on the x-axis and the outcome of the one step RT-qPCR assay (Log_{10} gc/mL) on the y-axis for the same viral solution (**Supplementary Fig. 6**). The calibration curve was used to determine the reliable range of the binding assay. The calibration curve for the binding assay was linear (a slope=0.95 and R^2=1.00) between 10^3 and 10^7 PFU/mL. The PCR standard curves were obtained with 10-fold serial dilutions of the synthetic DNA oligonucleotide (Integrated DNA technologies, USA) and the PCR efficiency for this one-step RT-qPCR ranged from 85 to 95% (R^2>0.99). Inhibitory effect of GSE was also tested (**Supplementary Fig. 7**). We found 100-fold dilution can reduce the inhibitory effect of GSE to an insignificant level, so the samples were diluted in molecular grade water by 100-fold before the RT-qPCR analysis. Information for RT-qPCR was summarized following the MIQE guidelines (52) in **Supplementary Table 4**.

Molecular docking simulation for polyphenols and capsid proteins interaction

We selected nine polyphenolic compounds that are present in GSE, including two phenolic acids, three monomer flavan-3-ols, and four dimer flavan-3-ols (36). The structural information on the polyphenols were obtained from PUBChem (https://pubchem.ncbi.nlm.nih.gov/). Although we conducted inactivation experiments with Tulane virus, we obtained HuNoV capsid protein instead of TV from the Protein Data Bank (PDB, https://www.rcsb.org/) to study interactions with the polyphenols because the database of

PDB does not provide TV capsid information. Cryo-EM structure analysis showed that the TV capsid structure closely resembles that of HuNoV(31).

We downloaded the HuNoV icosahedral asymmetric unit (PDB ID: 1IHM) which is a basic building block for the HuNoV capsid. This icosahedral unit comprised three VP1 proteins (i.e., chain A, B, and C in PDB format). The complete HuNoV capsid consists of 180 identical icosahedral asymmetric units. We also used a deep-learning-based structure prediction tool - trRosetta(53), to predict the 3D-structure of the TV capsid (**Supplementary File 1**) from its sequence and a multiple-sequence alignment of related sequences. We studied molecular docking of the polyphenols to HuNoV and to other different enteric viruses including hepatitis A virus (PDB: 4QPI), murine norovirus-1 (PDB: 6S6L), and feline calicivirus-F9 (PDB: 6GSH). Bovine serum albumin (BSA) is a major component for FBS, and BSA showed a strong binding affinity to the polyphenols as confirmed by the quenching effect in the virus inactivation experiments. BSA (PDB: 4F5S) was used as a positive control for molecular docking with the polyphenolic compounds. Next, we used the target proteins (capsids or BSA) and flexible conformations of all the aforementioned nine polyphenol ligands to discern stable docking conformations, record binding affinity scores, and report across four capsid domains where each of the polyphenols tend to bind in order of domain preference. The flexible docking protocol is similar to the Z-Dock protocol(37) as implemented within OptMAVEn-2.0(38).

Statistical analysis

All experiments were repeated three times with distinct virus samples (i.e., three biological replications), each of which was analyzed by three separate RT-qPCR measurements (i.e., three technical replications). Paired sample t-test was used to compare results of plaque assay and

554 aggregation assay in **Fig. 2C** and binding energies of different viral species (HuNoV, FCV,
555 MNV, and HAV) to polyphenolic compounds in **Fig. 6**. We confirmed that all data for statistical
556 analysis satisfied assumptions of paired sample t-test (i.e., no outliers and normality). For
557 example, all data for statistical analysis were between Q1-1.5IQR and Q3+1.5IQR range, which
558 means there were no outliers. Also, differences between two data sets (e.g., plaque assay versus
559 aggregation assay in **Fig. 2C** or HuNoV versus MNV or HAV in **Fig. 6**) were normally
560 distributed ($P>0.05$).
561

562 **Acknowledgement**

563 This study was funded by National Science Foundation (Award Number: 2023248). We thank
564 Dr. Zhong (Lucas) Li at Metabolomics Lab, Roy J. Carver Biotechnology Center, University of
565 Illinois at Urbana-Champaign for characterizing polyphenolic compounds in grape seed extract.
566

References

1. Ahmed SM, Hall AJ, Robinson AE, Verhoef L, Premkumar P, Parashar UD, Koopmans M, Lopman BA. 2014. Global prevalence of norovirus in cases of gastroenteritis: A systematic review and meta-analysis. Lancet Infect Dis 14:725–730.

2. Scallan E, Hoekstra RM, Angulo FJ, Tauxe R V., Widdowson MA, Roy SL, Jones JL, Griffin PM. 2011. Foodborne illness acquired in the United States-Major pathogens. Emerg Infect Dis 17:7–15.

3. Burke RM, Mattison CP, Pindyck T, Dahl RM, Rudd J, Bi D, Curns AT, Parashar U, Hall AJ. 2020. Burden of Norovirus in the United States, as Estimated Based on Administrative Data: Updates for Medically Attended Illness and Mortality, 2001–2015. Clin Infect Dis https://doi.org/10.1093/cid/ciaa438.

4. BITLER EJ, MATTHEWS JE, DICKEY BW, EISENBERG JNS, LEON JS. 2013. Norovirus outbreaks: a systematic review of commonly implicated transmission routes and vehicles. Epidemiol Infect 141:1563–1571.

5. Fraisse A, Temmam S, Deboosere N, Guillier L, Delobel A, Maris P, Vialette M, Morin T, Perelle S. 2011. Comparison of chlorine and peroxyacetic-based disinfectant to inactivate Feline calicivirus, Murine norovirus and Hepatitis A virus on lettuce. Int J Food Microbiol 151:98–104.

6. GIRARD M, NGAZOA S, MATTISON K, JEAN J. 2010. Attachment of Noroviruses to Stainless Steel and Their Inactivation, Using Household Disinfectants. J Food Prot 73:400–404.

7. Fuzawa M, Araud E, Li J, Shisler JL, Nguyen TH. 2019. Free Chlorine Disinfection Mechanisms of Rotaviruses and Human Norovirus Surrogate Tulane Virus Attached to

Fresh Produce Surfaces. Environ Sci Technol 53:11999–12006.

8. Chen X, Hung YC. 2016. Predicting chlorine demand of fresh and fresh-cut produce based on produce wash water properties. Postharvest Biol Technol 120:10–15.

9. Parish ME, Beuchat LR, Suslow T V., Harris LJ, Garrett EH, Farber JN, Busta FF. 2003. Methods to reduce/ eliminate pathogens from fresh and fresh-cut produce. Compr Rev Food Sci Food Saf 2:161–173.

10. Soto Beltran M, Jimenez Edeza M, Viera C, Martinez CI, Chaidez C. 2013. Sanitizing alternatives for Escherichia coli and Salmonella typhimurium on bell peppers at household kitchens. Int J Environ Health Res 23:331–341.

11. Matulonga B, Rava M, Siroux V, Bernard A, Dumas O, Pin I, Zock JP, Nadif R, Leynaert B, Le Moual N. 2016. Women using bleach for home cleaning are at increased risk of non-allergic asthma. Respir Med 117:264–271.

12. Cleveland J, Montville TJ, Nes IF, Chikindas ML. 2001. Bacteriocins: Safe, natural antimicrobials for food preservation. Int J Food Microbiol. Elsevier.

13. Devlieghere F, Vermeiren L, Debevere J. 2004. New preservation technologies: Possibilities and limitations, p. 273–285. *In* International Dairy Journal. Elsevier.

14. Joshi SS, Su X, D'Souza DH. 2015. Antiviral effects of grape seed extract against feline calicivirus, murine norovirus, and hepatitis A virus in model food systems and under gastric conditions. Food Microbiol 52:1–10.

15. Market analysis report. 2019. Polyphenols Market Size, Share & Trends Analysis Report By Product (Grape Seed, Green Tea, Cocoa), By Application (Beverages, Food, Feed, Dietary Supplements, Cosmetics), And Segment Forecasts, 2019 - 2025.

16. Memar MY, Adibkia K, Farajnia S, Kafil HS, Yekani M, Alizadeh N, Ghotaslou R. 2019.

The grape seed extract: A natural antimicrobial agent against different pathogens. Rev Med Microbiol 30:173–182.

17. D'Souza DH. 2014. Phytocompounds for the control of human enteric viruses. Curr Opin Virol 4:44–49.

18. Su X, D'Souza DH. 2011. Grape seed extract for control of human enteric viruses. Appl Environ Microbiol 77:3982–3987.

19. Su X, D'Souza DH. 2013. Grape seed extract for foodborne virus reduction on produce. Food Microbiol 34:1–6.

20. Farkas T, Sestak K, Wei C, Jiang X. 2008. Characterization of a Rhesus Monkey Calicivirus Representing a New Genus of Caliciviridae. J Virol 82:5408–5416.

21. Zhang D, Huang P, Zou L, Lowary TL, Tan M, Jiang X. 2015. Tulane Virus Recognizes the A Type 3 and B Histo-Blood Group Antigens. J Virol 89:1419–1427.

22. Tan M, Wei C, Huang P, Fan Q, Quigley C, Xia M, Fang H, Zhang X, Zhong W, Klassen JS, Jiang X. 2015. Tulane virus recognizes sialic acids as cellular receptors. Sci Rep 5:1–14.

23. Bridges DF, Breard A, Lacombe A, Valentine DC, Tadepalli S, Wu VCH. 2017. Inhibition of Tulane Virus replication via exposure to lowbush blueberry (Vaccinium angustifolium) fractional components. J Berry Res 7:281–289.

24. Li X, Huang R, Chen H. 2017. Evaluation of Assays to Quantify Infectious Human Norovirus for Heat and High-Pressure Inactivation Studies Using Tulane Virus. Food Environ Virol 9:314–325.

25. Ailavadi S, Davidson PM, Morgan MT, D'Souza DH. 2019. Thermal Inactivation Kinetics of Tulane Virus in Cell-Culture Medium and Spinach. J Food Sci 84:557–563.

636 26. Araud E, Fuzawa M, Shisler JL, Li J, Nguyen TH. 2020. UV inactivation of rotavirus and
637 tulane virus targets different components of the virions. Appl Environ Microbiol 86:1–12.
638 27. Fuzawa M, Bai H, Shisler JL, Nguyen TH. 2020. The basis of peracetic acid (PAA)
639 inactivation mechanisms for rotavirus and Tulane virus under conditions relevant for
640 vegetable sanitation. Appl Environ Microbiol 1–47.
641 28. Ho YS, McKay G. 1999. Pseudo-second order model for sorption processes. Process
642 Biochem 34:451–465.
643 29. Ho YS, Ng JCY, McKay G. 2001. Removal of lead(II) from effluents by sorption on peat
644 using second-order kinetics. Sep Sci Technol 36:241–261.
645 30. Ho YS, Ofomaja AE. 2006. Pseudo-second-order model for lead ion sorption from
646 aqueous solutions onto palm kernel fiber. J Hazard Mater 129:137–142.
647 31. Yu G, Zhang D, Guo F, Tan M, Jiang X, Jiang W. 2013. Cryo-EM Structure of a Novel
648 Calicivirus, Tulane Virus. PLoS One 8:59817.
649 32. Pianet I, André Y, Ducasse M-A, Tarascou I, Lartigue J-C, Pinaud N, Fouquet E, Dufourc
650 EJ, Laguerre M. 2008. Modeling Procyanidin Self-Association Processes and
651 Understanding Their Micellar Organization: A Study by Diffusion NMR and Molecular
652 Mechanics. Langmuir 24:11027–11035.
653 33. Islam B, Sharma C, Adem A, Aburawi E, Ojha S. 2015. Insight into the mechanism of
654 polyphenols on the activity of HMGR by molecular docking. Drug Des Devel Ther
655 9:4943–4951.
656 34. Srinivasan E, Rajasekaran R. 2016. Computational investigation of curcumin, a natural
657 polyphenol that inhibits the destabilization and the aggregation of human SOD1 mutant
658 (Ala4Val). RSC Adv 6:102744–102753.

659 35. Chedea VS, Echim C, Braicu C, Andjelkovic M, Verhe R, Socaciu C. 2011. Composition
660 in polyphenols and stability of the aqueous grape seed extract from the romanian variety
661 “merlot recas.” J Food Biochem 35:92–108.
662 36. Rodríguez Montealegre R, Romero Peces R, Chacón Vozmediano JL, Martínez Gascueña
663 J, García Romero E. 2006. Phenolic compounds in skins and seeds of ten grape Vitis
664 vinifera varieties grown in a warm climate. J Food Compos Anal 19:687–693.
665 37. Pierce BG, Hourai Y, Weng Z. 2011. Accelerating protein docking in ZDOCK using an
666 advanced 3D convolution library. PLoS One 6.
667 38. Chowdhury R, Allan MF, Maranas CD. 2018. OptMAVEn-2.0: De novo Design of
668 Variable Antibody Regions Against Targeted Antigen Epitopes. Antibodies 7:23.
669 39. Campillay-Véliz CP, Carvajal JJ, Avellaneda AM, Escobar D, Covián C, Kalergis AM,
670 Lay MK. 2020. Human Norovirus Proteins: Implications in the Replicative Cycle,
671 Pathogenesis, and the Host Immune Response. Front Immunol. Frontiers Media S.A.
672 40. Cosconati S, Forli S, Perryman AL, Harris R, Goodsell DS, Olson AJ. 2010. Virtual
673 screening with AutoDock: Theory and practice. Expert Opin Drug Discov. NIH Public
674 Access.
675 41. Chaudhury S, Lyskov S, Gray JJ. 2010. PyRosetta: A script-based interface for
676 implementing molecular modeling algorithms using Rosetta. Bioinformatics. Oxford
677 Academic.
678 42. Soares S, Mateus N, De Freitas V. 2007. Interaction of different polyphenols with Bovine
679 Serum Albumin (BSA) and Human Salivary α-Amylase (HSA) by fluorescence
680 quenching. J Agric Food Chem 55:6726–6735.
681 43. Johnson M. 2012. Fetal Bovine Serum. Mater Methods 2.

682 44. Bultmann H, Busse JS, Brandt CR. 2001. Modified FGF4 Signal Peptide Inhibits Entry of
683 Herpes Simplex Virus Type 1. J Virol 75:2634–2645.
684 45. Lodder WJ, De Roda Husman AM. 2005. Presence of noroviruses and other enteric
685 viruses in sewage and surface waters in The Netherlands. Appl Environ Microbiol
686 71:1453–1461.
687 46. Rutjes SA, Lodder WJ, Van Leeuwen AD, De Roda Husman AM. 2009. Detection of
688 infectious rotavirus in naturally contaminated source waters for drinking water production.
689 J Appl Microbiol 107:97–105.
690 47. Cromeans T, Park GW, Costantini V, Lee D, Wang Q, Farkas T, Lee A, Vinjé J. 2014.
691 Comprehensive comparison of cultivable norovirus surrogates in response to different
692 inactivation and disinfection treatments. Appl Environ Microbiol 80:5743–5751.
693 48. Dunkin N, Weng S, Schwab KJ, McQuarrie J, Bell K, Jacangelo JG. 2017. Comparative
694 Inactivation of Murine Norovirus and MS2 Bacteriophage by Peracetic Acid and
695 Monochloramine in Municipal Secondary Wastewater Effluent. Environ Sci Technol
696 51:2972–2981.
697 49. Oguma K, Kita R, Sakai H, Murakami M, Takizawa S. 2013. Application of UV light
698 emitting diodes to batch and flow-through water disinfection systems. Desalination
699 328:24–30.
700 50. Araud E, DiCaprio E, Ma Y, Lou F, Gao Y, Kingsley D, Hughes JH, Li J. 2016. Thermal
701 inactivation of enteric viruses and bioaccumulation of enteric foodborne viruses in live
702 oysters (Crassostrea virginica). Appl Environ Microbiol 82:2086–2099.
703 51. Dong S, Li J, Kim MH, Park SJ, Eden JG, Guest JS, Nguyen TH. 2017. Human health
704 trade-offs in the disinfection of wastewater for landscape irrigation: Microplasma

ozonation: Vs. chlorination. Environ Sci Water Res Technol 3:106–118.

52. Bustin SA, Benes V, Garson JA, Hellemans J, Huggett J, Kubista M, Mueller R, Nolan T, Pfaffl MW, Shipley GL, Vandesompele J, Wittwer CT. 2009. The MIQE guidelines: Minimum information for publication of quantitative real-time PCR experiments. Clin Chem 55:611–622.

53. Yang J, Anishchenko I, Park H, Peng Z, Ovchinnikov S, Baker D. 2020. Improved protein structure prediction using predicted interresidue orientations. Proc Natl Acad Sci U S A 117:1496–1503.